Article

Patterns

Guiding maps of solvents for lithium-sulfur batteries via a computational data-driven approach

Graphical abstract

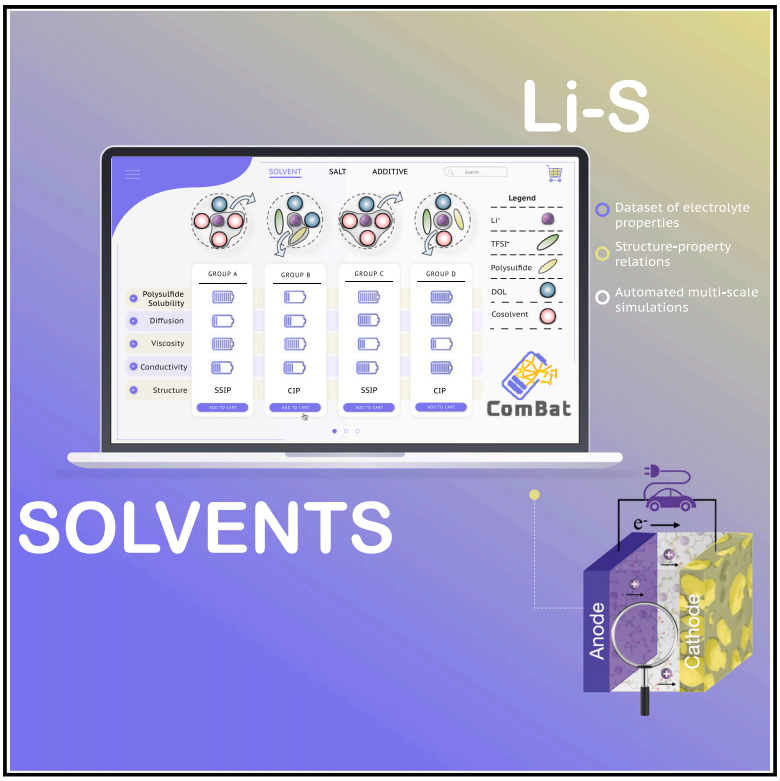

Highlights

- ComBat database provides insights for optimal Li-S electrolytes
- Molecular-level interactions drive ion dissociation and electrochemical performance
- A new quantitative metric classifies Li-S solvents based on diffusion mechanism
- The accompanying open-source code ensures full reproducibility of this work

Authors

Rasha Atwi, Nav Nidhi Rajput

Correspondence

navnidhi.rajput@stonybrook.edu

In brief

This study introduces ComBat, an extensive database for designing optimal lithium-sulfur (Li-S) battery electrolytes. By employing computational chemistry to scrutinize molecular-level interactions, the authors uncover the complex interplay of factors dictating polysulfide solubility and ion dissociation. The insights gained from ComBat can expedite the development of advanced Li-S electrolytes, addressing the need for next-generation energy storage devices. The open-source nature of ComBat and the underlying code ensures full reproducibility, making it a valuable resource for the electrochemical and materials science community.

Atwi & Rajput, 2023, Patterns *4*, 100799
September 8, 2023
https://doi.org/10.1016/j.patter.2023.100799

CellPress

Patterns

CellPress
OPEN ACCESS

Article

Guiding maps of solvents for lithium-sulfur batteries via a computational data-driven approach

Rasha Atwi[1] and Nav Nidhi Rajput[1,2,*]
[1]Department of Materials Science and Chemical Engineering, Stony Brook University, Stony Brook, NY 11794, USA
[2]Lead contact
*Correspondence: navnidhi.rajput@stonybrook.edu
https://doi.org/10.1016/j.patter.2023.100799

THE BIGGER PICTURE The need for advanced energy storage technologies has led to growing interest in lithium-sulfur (Li-S) batteries due to their high theoretical capacity and energy density. However, practical application is hindered by a short life cycle and low-rate capability, traceable to electrolyte instability. Limited systematic studies on molecular mechanisms governing Li-S electrolyte behavior hinder the development of optimized electrolyte compositions. This work introduces ComBat, a comprehensive database providing insights into molecular-level interactions among solvent, salt, and polysulfide species in Li-S batteries. By combining quantum-chemical and molecular dynamics simulations, we investigate critical electrolyte properties such as binding affinities and diffusion mechanisms. ComBat is a valuable resource for systematic, knowledge-driven design of high-performance electrolytes for advanced Li-S batteries.

Development/Pre-production: Data science output has been rolled out/validated across multiple domains/problems

SUMMARY

Practical realization of lithium-sulfur batteries requires designing optimal electrolytes with controlled dissolution of polysulfides, high ionic conductivity, and low viscosity. Computational chemistry techniques enable tuning atomistic interactions to discover electrolytes with targeted properties. Here, we introduce ComBat (Computational Database for Lithium-Sulfur Batteries), a public database of ~2,000 quantum-chemical and molecular dynamics properties for lithium-sulfur electrolytes composed of solvents spanning 16 chemical classes. We discuss the microscopic origins of polysulfide clustering and the diffusion mechanism of electrolyte components. Our findings reveal that polysulfide solubility cannot be determined by a single solvent property like dielectric constant. Rather, observed trends result from the synergistic effect of multiple factors, including solvent C/O ratio, fluorination degree, and steric hindrance effects. We propose binding energy as a proxy for Li^+ dissociation, which is a property that impacts the ionic conductivity. The insights obtained in this work can serve as guiding maps to design optimal lithium-sulfur electrolyte compositions.

INTRODUCTION

Lithium-ion (Li-ion) batteries have come to be the most prominent battery technology for portable electronic devices and electric vehicles.[1–3] Still, development of alternative battery chemistries is urgently needed to satisfy the ever-growing energy storage demands.[2] Among various proposed avenues toward this goal, lithium-sulfur (Li-S) batteries are recognized as one of the most promising next-generation electrochemical energy storage systems, owing to their low cost and high energy density.[4] The Li metal anode based on the stripping/plating mechanism can provide a high theoretical specific capacity of 3,860 mAh g^{-1}.[5] Meanwhile, the multi-electron conversion chemistry at the cost-efficient S cathode also leads to a high theoretical specific capacity of 1,675 mAh g^{-1}.[5] The result is a cell with the prospect of ultrahigh theoretical gravimetric energy density of 2,510 Wh kg^{-1}, much higher than conventional Li-ion batteries (387 Wh kg^{-1}).[2,6]

Practical realization of this high energy density in Li-S batteries, however, is constrained by the detrimental shuttle effect

originating from dissolution of lithium polysulfides (Li_2S_x; x = 4–8) during cycling and the electrical insulating properties of elemental sulfur and the solid reduction products (Li_2S and Li_2S_2).[7] Severe shuttle phenomena cause poor utilization of active materials, fast self-discharge, infinite charge, low Coulombic efficiency (CE), increased internal resistance, and rapidly diminishing capacity.[2,6] Many of these challenges are related to the nature and properties of the Li-S electrolyte. The composition and stability of the solid-electrolyte interphase (SEI) layer is also inherently dependent on the electrolyte and its intimate interaction with the Li anode.[8,9] Thus, designing electrolytes with reduced solubility of high-order Li_2S_x is of great significance for controlling the deleterious side reactions and protecting the electrode surface. Such a strategy may complement significant efforts in composite particle design aimed at confining elemental sulfur and anchoring the polysulfides.[10–12] Other desired electrolyte properties include high ionic conductivity, low viscosity, high chemical stability, and compatibility with the electrodes.

Liquid electrolytes composed of organic solvents, Li salt, such as lithium bis(trifluoromethne sulfone) imide (LiTFSI) or lithium bis(fluorosulfonyl) imide (LiFSI), and an additive, such as lithium nitrate ($LiNO_3$), dominate the mainstream due to their high ionic conductivity.[2,13] The selection of solvent in particular plays a crucial role in the transportation of ions and determines the polysulfide solubility and the Li anode stability. Liquid organic Li-S electrolyte solvent demonstrations have gone through a process from aliphatic amines to carbonates and then to ethers. Special attention has been given to cyclic or linear "ethers," such as tetrahydrofuran (THF), 1,3-dioxolane (DOL), dimethoxyethane (DME), and tetra(ethylene glycol)-dimethyl ether (TEGDME), owing to their lower vulnerability to nucleophilic attack from S^- centers compared with carbonates.[6] The most widely used Li-S electrolyte comprises ~1 M LiTFSI salt in a binary DOL/DME (1/1, v/v) solvent mixture with 1–2 wt % $LiNO_3$.[14] This electrolyte formulation suffers, however, from the high dissolution of high-order Li_2S_x species, which facilitates the shuttle process and subsequent parasitic reactions.[15] Therefore, several alternative Li-S solvent classes were introduced recently.

Among the newly proposed electrolytes, "fluorinated" ether solvents have received growing interest due to the high electronegativity of fluorine, low melting point, low Li_2S_x solubility, and ability to build a stable passivation layer on the anode.[16–18] Several studies reported lower self-discharge rates with the use of fluorinated co-solvents, but they come at the expense of low Li salt solubility, necessitating the use of co-solvents in the electrolyte systems.[19–21] "Sulfone"-based electrolytes have been applied in Li-S batteries due to their favorable oxidative stability and dielectric constant.[22–24] However, they are usually mixed with ethers to balance their high viscosity and polysulfide solubility.[22] Recently, a localized low concentration electrolyte (LLCE) composed of a binary mixture of fluorinated and sulfone-based co-solvents has been applied to an Li-S cell, showing great promise in polysulfide suppression, reduced viscosity, and high capacity.[25] Wang et al. have reported the use of "phosphate" and "phosphite" solvents, such as trimethyl phosphate (TMP)[26] and tris(2,2,2-trifluoroethyl) phosphite (TTFP),[27] as co-solvents with carbonates to form an effective flame-retardant electrolyte. Additionally, they developed a novel intrinsic flame-retardant electrolyte consisting of a mixture of TMP and a fluorinated co-solvent, 1,1,2,2-tetra-fluoroethyl-2,2,3,3-tetrafluoropropyl ether (TTE), which enables a high CE, stable, and dendrite-free cycling with Li metal anode.[26] Another successfully applied electrolyte system is a "nitrile"-based (acetonitrile [ACN]) sparingly solvating electrolyte with a fluorinated co-solvent.[28] The synergistic effect of the nitrile and fluorinated solvents limits the dissolution and mobility of polysulfides while maintaining viscosities that approach that of conventional ethers.

Despite the significant body of work on Li-S electrolyte systems, there is much that is still not understood in terms of the structure-property relationships of electrolytes and the contribution of the speciation to the overall ionic transport properties. Since it is also unlikely for a single solvent to fulfill all the performance metrics of an Li-S electrolyte, understanding how the solvent affects the solvation structure, and thus the electrolyte properties, is of utmost importance to establish design principles that ultimately allow their smart design and optimization (e.g., choice of the composition of binary or ternary solvent mixtures). Driven by these needs, we seek to understand how the replacement of DME in the state-of-the art solvent mixture of DOL:DME with different classes of commonly reported Li-S solvents alters the structure and dynamics of Li-S electrolytes. To do so, we leverage our recently developed high-throughput multi-scale computational framework[29,30] (MISPR: materials informatics for structure-property relationships); https://github.com/molmd/mispr) to construct a database of Li-S electrolyte properties from a series of automated density functional theory (DFT) and classical molecular dynamics (CMD) simulations. The publicly available dataset—Computational Database for Li-S Batteries (ComBat)[31]—contains ~2,000 properties of 56 Li-S electrolyte systems spanning 16 different chemical classes that have been previously reported in experimental Li-S studies (see Figure 1). The dataset provides crucial atomistic-level insight of various properties, including equilibrated configurations, solvation structures, diffusion coefficients, ionic conductivities, viscosities, radial distribution functions, coordination numbers, and polysulfide clustering. We use the ComBat database to highlight the unique behavior of each co-solvent class, develop a quantitative model for the primary speciation in solution and its relation to the dynamics, and unravel the underpinnings governing the polysulfide dissolution. We find that there is no single descriptor that explains the trends in the polysulfide solubility. We anticipate that this work will serve two purposes: (1) provide fundamental insights from a scientific basis for the understanding of Li-S electrolytes to accelerate their development and achieve parity with lithium-ion electrolytes, and (2) demonstrate the capacity of our high-throughput computational framework for predicting atomistic properties of electrolytes for a large chemical space.

RESULTS AND DISCUSSION

Overview of the ComBat database

The set of 56 co-solvents was built to adequately cover molecules reported in common Li-S electrolytes used in experimental studies. Representation of the co-solvents are provided in Table S1. These co-solvents can be grouped into 16 chemical classes: acetamide (1–2), acetate (3), azole (4–5), ether (6–19),

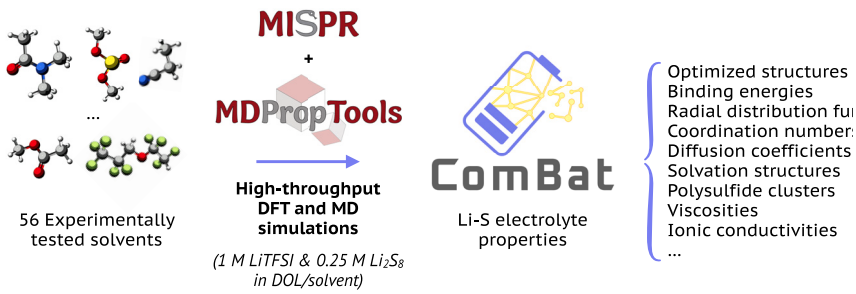

Figure 1. Overview of the ComBat database
Selected DFT- and CMD-computed properties in the ComBat database for electrolyte mixtures composed of 1 M LiTFSI and 0.25 M Li_2S_8 in DOL/solvent. Calculations are performed using the MISPR infrastructure for high-throughput coupled DFT-CMD simulations and MDPropTools for analysis of simulation trajectories.

fluorinated (20–36), formamide (37), nitrile (38–39), nonpolar (40–41), phosphate (42–43), phosphite (44), silane (45), sulfide (46), sulfite (47–48), sulfonamide (49–50), sulfone (51–55), and sulfoxide (56). The solvents were retrieved from the PubChem database.[32] While Figure S1A shows selected small molecules in the ComBat dataset, the distribution of solvent sizes (in terms of the number of electrons) is wide with a range between 22 and 162 electrons. We further note that a large number of molecules in the database belong to the C-H-O chemical system, but many fluorine-, sulfur-, and nitrogen-containing molecules are included as well (Figure S1B). The diversity in phosphorous- and silicon-containing molecules is lacking because only a few solvents with these elements have been explored so far. Considering that many chemical classes and the most reported solvents are considered in the ComBat dataset, we believe the dataset is broad enough to capture a sufficiently diverse range of structural/dynamical properties to be used to create accurate models for Li-S electrolytes.

While many electrolyte chemistries have been developed for Li-S batteries, the most widely used formulation consists of 1 M LiTFSI in DOL/DME (1/1, v/v). To understand the effect of solvents on the properties of Li-S electrolytes, we systematically considered two sets of electrolyte systems: (1) 1 M LiTFSI, 0.25 M Li_2S_8 in DOL/co-solvent (1/1, v/v), and (2) 1 M LiTFSI in DOL/co-solvent (1/1, v/v), leading to a total of 112 modeled electrolyte systems. A detailed analysis of structural and dynamical properties (e.g., radial distribution function [RDF], coordination number [CN], diffusion, clustering, …) was performed using the first set while the ionic conductivity and viscosity calculations were performed using the second set. We further note that while DME is known to provide high ionic conductivity due to its ability to dissociate the salts, it is the main culprit behind the high polysulfide solubility in Li-S battery electrolytes. Therefore, in this work we replaced DME in the state-of-the-art electrolyte instead of DOL. At the current stage, ComBat contains properties relevant to these electrolytes, but does not necessarily consider the exact electrolyte compositions used in Li-S literature. For example, while DMSO was previously used as a unary solvent to dissolve 1 M LiTFSI,[33–36] it was mixed in an equivolume mixture with DOL in this work to ensure consistency across our electrolyte systems for comparison purposes. We anticipate that the set will be extended with future systematic studies to include other anions, additives, and polysulfide chain lengths, and updates will be made available at https://github.com/rashatwi/combat. Methodological details regarding the dataset construction, DFT calculations, CMD simulations, and analysis can be found in the supplemental information.

Binding energy as a descriptor for solvent coordinating power

One strategy to achieve solubility and mobility of the supporting salt and not polysulfides and create a degree of selective solvation is to tune the solvent solvating power. As shown in Figure 2, the chemical class and type of the solvent modify the binding energy and thus its coordinating ability to the ligand, i.e., Li^+ of LiTFSI and Li_2S_8. Overall, solvents of the same chemical class exhibit similar orders of binding energy and degrees of Li^+ dissociation (represented through the size of the scatter points in Figure 2). Li^+ dissociation is defined as the population of Li^+ ions that do not have S_8^{2-} in their solvation shells. The degree of solvating power ranges from the completely solvating ether-based solvent TEGDME to the completely non-solvating silane-based solvent trifluoromethyl trimethyl silane (TFMTMS). On average, a positive correlation is observed between the binding affinity and the degree of Li^+ dissociation. In general, dissociation is highest in systems containing a strongly coordinating solvent, such as sulfone-, sulfoxide-, and azole-based solvents, and lowest in systems containing a weakly coordinating solvent, such as nonpolar-, fluorinated-, and silane-based solvents. The dissociation and binding energies with TEGDME and triglyme (G3) are noticeably different from the rest of the ether solvents due to their ability to wrap around the ligands in a more energetically favorable conformation. Similarly, 1-(2,2,2-trifluoroethoxy)-2-methoxyethane (TFEG), 1,1,2,2-tetrafluoro-3-(2-methoxyethoxy) propane (TFPG), and 1,1,1,8,8,8-hexafluoro-3,6-dioxaoctane (DTFEG) are characterized with higher Li^+ dissociation and binding affinities than other fluorinated solvents in the Li-S dataset, which can likely be attributed to the presence of more than one oxygen coordinating site and the farther proximity of these oxygen atoms from the fluorine sites.

It has been suggested that the dissolution of a small amount of polysulfides can promote the complete reduction of sulfur and improve the sulfur utilization rate.[37,38] TTE does not solubilize polysulfides at room temperature, while DME binds strongly to the cation and dissolves polysulfides.[17] Area 1 in Figure 2 presents a "sweet spot" where the interactions with Li_2S_8 are stronger than those of TTE but weaker than those of conventional DME. Thus, solvents in Area 1 can be used as selective co-solvents with optimal cation dissociation. Area 2 constitutes solvents whose Li_2S_8 binding affinities are lower than that of TTE and result in limited Li^+ dissociation that diminishes the electrolyte conductivity. These solvents are best used as diluents to decrease the overall polysulfide solubility without altering the electrolyte structural properties. We lastly note that binding energy is a molecular property obtained from DFT calculations of individual solvent molecules and ligands. In contrast, the fraction

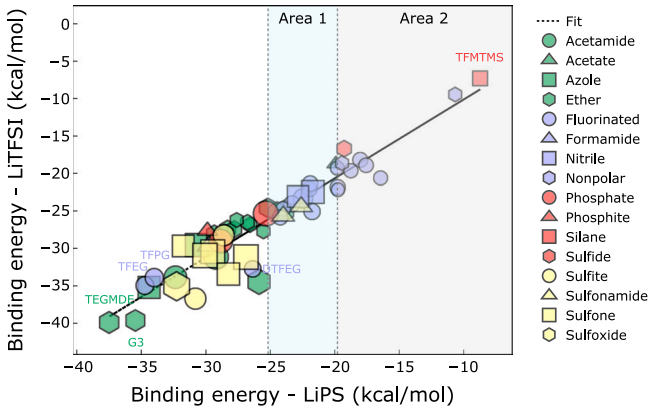

Figure 2. Binding affinities from DFT calculations

Binding energy of solvents in the Li-S dataset with LiTFSI and Li_2S_8 (LiPS) including the degree of Li^+ dissociation from S_8^{2-} (indicated by the size of the scatter points). Area 1 corresponds to solvents whose binding affinity with Li_2S_8 is higher than TTE but lower than that of DME while Area 2 consists of solvents that do not dissolve polysulfides. An interactive plot is hosted on GitHub at https://rashatwi.github.io/combat/plots/be.html.

of dissociated Li^+ from polysulfides is an ensemble property obtained from fully equilibrated electrolyte mixtures using CMD simulations. The revealed correlation between these two properties together with the affordable computational cost of binding energy calculations make binding energy an effective descriptor in fast screening computational studies aimed at finding new potential solvent candidates.

Structure of the lithium solvation shell

Next, we investigate the structure of the lithium solvation shell as a function of the type of the co-solvent in electrolytes composed of 1 M LiTFSI and 0.25 M Li_2S_8 in DOL/co-solvent (1/1, v/v). Figure 3A shows the RDF $g(r)$ for Li^+ - X (Solvent), Li^+ - O (DOL), Li^+ - O (TFSI), Li^+ - S (PS), and Li^+ - Li^+ in selected electrolyte systems from each co-solvent chemical class. Similar plots for the full Li-S dataset are shown in Figures S3 and S4 along with the type of the co-solvent coordinating sites X used in $g(r)$ calculations. Figure 3B shows the average number of coordinating atoms from the electrolyte components in the first solvation shell of the cation. For the electrolytes investigated in this work, the total coordination number of Li^+ varies between 3.9 and 5.7. In most electrolytes, the closest interaction with Li^+ occurs with the co-solvent at ~1.9 Å. The Li^+ interactions with the cyclic ether DOL are much weaker than those with the co-solvent, which is mainly attributed to the lower structural flexibility of DOL molecules. The fluorinated, nonpolar, silane, and sulfide solvents are an exception to this behavior, as they scarcely participate in solvating Li^+, which is evident from the lack of an Li^+ - X (Solvent) $g(r)$ peak and their negligible coordination number with the metal cation (Figure 3B). Instead, DOL gets introduced to the primary Li^+ solvation shell in these systems at ~1.9 Å with a coordination number of Li^+ with oxygen atoms of DOL between 0.9 and 2.4. These systems are also characterized with the sharpest Li^+ - S (PS) peaks at a distance ~2.1 Å and the highest Li^+ - S (PS) coordination numbers indicating very strong electrostatic interactions between the cation and the polysulfides.

In all electrolytes, Li^+ interactions with S_8^{2-} occur at a farther distance (2.1 Å) than with other components, showcasing the flexibility of the polysulfides in accommodating Li^+ in their first solvation shell. Additionally, $g(r)$ signifying the Li^+ - Li^+ correlation (Figures S5 and S6) in fluorinated, nonpolar, silane, and sulfide systems exhibits two sharp peaks at 4.2 and 5.8 Å followed by a broader shoulder peak at 8.9 Å, indicating highly ordered long-range structures where S_8^{2-} acts as a bridge between Li^+ to form Li^+ … S … Li^+ ionic chains. The Li^+ - Li^+ peaks are less pronounced in systems characterized with strong Li^+ - solvent interactions signifying weak long-range structures such as Li^+-rich domains (see for example the Li^+ - Li^+ $g(r)$ in acetamide, azole, formamide, and nitrile systems in Figures S5 and S6). These systems are also characterized with the lowest Li^+ - Li^+ coordination numbers, as shown in Figure 3B. Interestingly, despite the strong interaction of DMSO with Li^+, the Li^+ - Li^+ $g(r)$ in this electrolyte exhibits a unique behavior where the first peak occurs at a close distance of 2.6 Å with high intensity, followed by a second peak at 7.3 Å, and a third broader peak at 14.1 Å (Figure S6).

The strong Li^+ - Li^+ interactions are driven by the bridging effect originating this time from the DMSO oxygen atom that brings two Li^+ ions to a shorter distance (see Figure S7A for a visual conformation of the bridging mechanism). Figure S7B shows that the oxygen atoms on the sulfone functional group also act as a bridge to bring two cations together according to Li^+ … O=S=O … Li^+, leading to the observed peaks in the Li^+ - Li^+ $g(r)$ and an average Li^+ - Li^+ coordination number of 1.4 in sulfone and sulfonamide electrolytes. Therefore, not only the polysulfide species but also the solvent molecules may contribute to the bridging effect. The bridging effect brought by the polysulfide species leads to significant agglomeration and the formation of well-defined domains in Li-S electrolytes, as evident from the snapshots in Figures S7C and S7D. Sample snapshots of these systems confirm that the fluorinated, nonpolar, silane, and sulfide solvents behave as anti-solvents with LiTFSI and Li_2S_8 being localized in the DOL-rich domains. The formed nanodomain structures and localization of S_8^{2-} are consistent with the reduced solubility of Li_2S_8 reported in these solvents[19,39–42] and are expected to facilitate the conversion of longer polysulfides to shorter sulfides.[25]

The phosphite solvent has a weaker solvating power compared with the phosphates because the coordinating oxygen sites in the latter are sterically less accessible than the doubly bonded oxygen site on the phosphates. Among the ether solvents, $g(r)$ corresponding to the *tert*-butyl methyl ether (MTBE), diisopropyl ether (DIPE), butyl ether (DBE), ethyl propyl ether (EPE), and 1-methoxyhexane (HME) systems are visibly distinct from the other ether-based systems in the ComBat dataset (Figure S3). Li^+ - O (Solvent) interactions in these systems are much weaker, which is mainly attributed to the higher solvent C/O ratio (Table S5) and the extra steric hindrance caused by branching in some of these solvent molecules. The weak solvating power of these solvents leads to stronger Li^+ - O ($TFSI^-$) and Li^+ - S (PS) interactions and higher possibility of forming contact ion pairs (CIPs) and aggregates (AGGs) in the electrolytes.

Among the fluorinated solvents, DTFEG, TFPG, and TFEG exhibit distinct behavior compared with other fluorinated

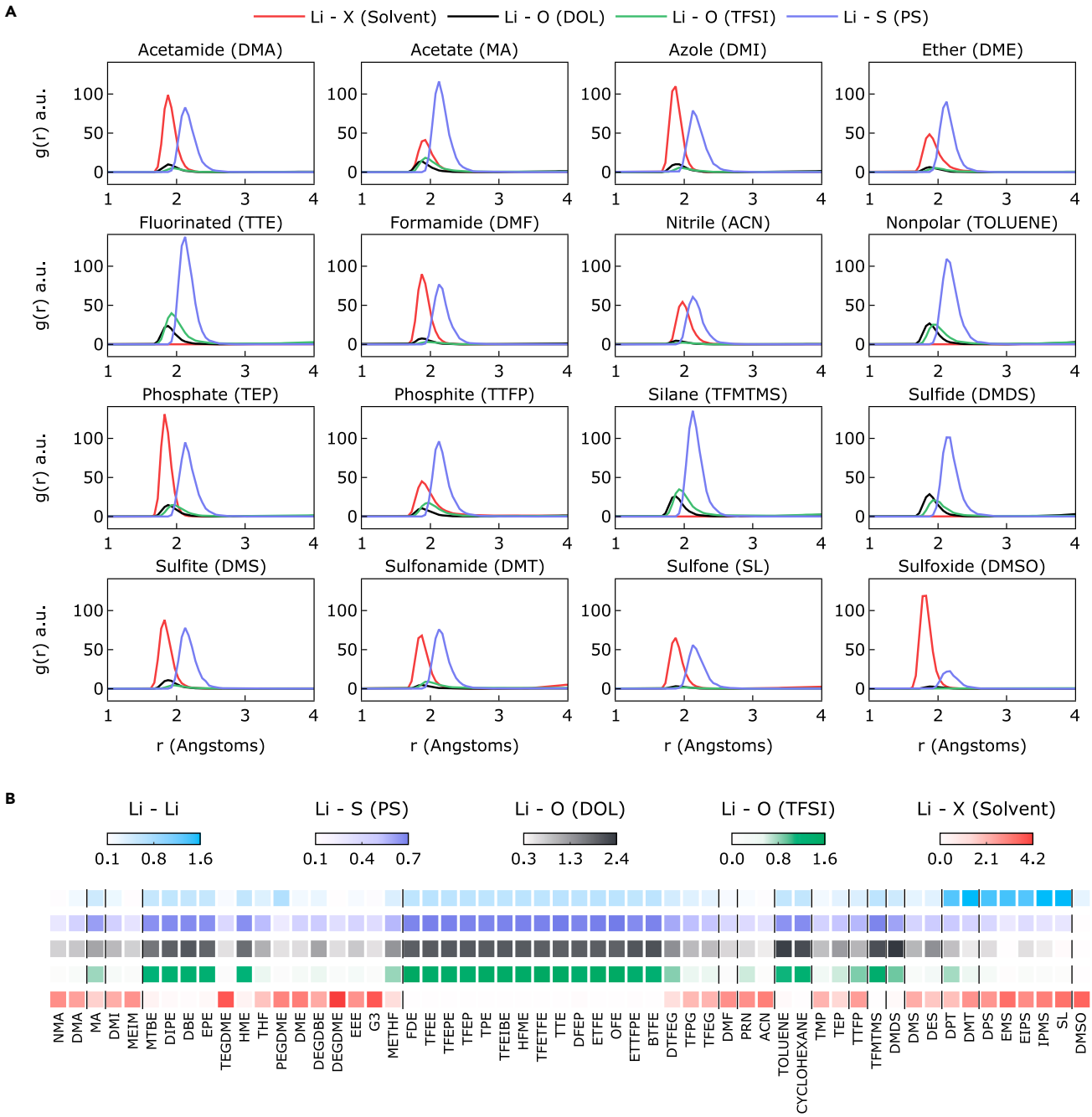

Figure 3. Structural analysis of selected electrolytes from the ComBat dataset

(A) Radial distribution function g(r) and (B) coordination number of Li^+ - X (Solvent), Li^+ - O (DOL), Li^+ - O ($TFSI^-$), and Li^+ - S (PS). Coordination numbers between two Li^+ ions are also included in the heatmaps. Darker colors indicate higher coordination numbers and stronger interactions, while lighter colors indicate lower coordination numbers and weaker interactions between Li^+ and the different electrolyte components.

solvents. This can be rationalized by the presence of multiple oxygen coordinating sites and the ability of these solvents to wrap around Li^+ and solvate it. Although 1,3-bis(1,1,2,2-tetrafluoroethoxy) propane (FDE) and 1,2-bis(1,1,2,2-tetrafluoroethoxy) ethane (TFEE) are also composed of two ether oxygen sites, the close vicinity of the coordinating oxygen sites to the electron-withdrawing fluorine groups limits the coordinating power of these solvent molecules. Alternatively, 1,1,2,2,3,3,4,4-octafluoro-5-(1,1,2,2-tetrafluoroethoxy) pentane (OFE) fluorinated solvent system is characterized with the sharpest Li^+ - S (PS) peak (Figure S4), which is caused by its highest fluorination degree (Table S6). Interestingly, triethyl phosphate (TEP) and TMP result in similar structural properties, as shown in Figure S4, despite the substantial difference in their dielectric constants

(ε_{TEP} = 12.94, ε_{TMP} = 21.26). On the other extreme, DIPE and N-methyl acetamide (NMA) have very similar dielectric constants (3.95 and 3.97, respectively), yet their solvating power is completely different. These observations indicate that the solvating power does not increase monotonically with the solvent dielectric constant but is rather the result of an intricate interplay among many additional factors, such as C/O ratio, fluorination degree, and steric hindrance effects.

Negligible Li^+ - $TFSI^-$ interactions are observed in systems containing acetate, formamide, nitrile, sulfite, sulfonamide, sulfone, sulfoxide, and some ether solvents, indicating the presence of solvent separated ion pairs (SSIPs). The salt in these systems is largely dissociated and well dispersed, as evident from the sample snapshot in Figure S8A. Nanometric aggregates (n-AGGs)[8] are observed in electrolytes with fluorinated, nonpolar, silane, and sulfide solvents, where the salt forms heterogeneous ion-rich domain networks (see Figure S8B). The formation of n-AGG structures in these electrolytes is driven by the stronger ion-ion electrostatic interactions than the ion-solvent interactions. These n-AGG structures are expected to add more complexity to the electrochemical redox, transport, and interfacial properties of the electrolyte.[8] Additionally, DOL and fluorinated solvents separate into two phases in fluorinated solvent-based electrolytes, giving rise to the "fluorous" effect.[43] Due to the low polarizability of C–F bonds, fluorous domains tend to have limited tendency to interact with other molecules in the electrolyte and thus aggregate into a separate phase (Figure S9).

The top four Li^+ solvation structures and their probability of occurrence obtained from our simulations are provided in Figures S10 and S11, and Tables S7–S10. Overall, we find that there is no single dominant solvation structure, as evident from the low probability of the top structure in each system. Structures identified in the high dielectric constant solvents EMS (ε_{EMS} = 57.5), SL (ε_{SL} = 44.0), and DMSO (ε_{EMS} = 46.5) are an exception to this behavior. In these systems, the cation is persistently coordinated by four co-solvent molecules giving rise to SSIPs or free ions at a probability between 42% and 63%. Although high Li^+ dissociation is desired to achieve the high ionic conductivity needed to support high current density, the strong binding of the cation to the solvents reduces the Li-ion transference number.[44,45] Additionally, the high dielectric constant of the solvents inevitably increases the dipole-dipole forces among the solvent molecules, thereby increasing their freezing temperature and reducing the low-temperature performance of the electrolytes.[44,46] The four-coordinated $[Li(DOL)_2(TFSI)_1(S_8)_1]^{2-}$ cluster exists as a common top solvation structure in low dielectric constant ethers, fluorinated, nonpolar, and silane solvents, indicating that these solvents do not participate in primary solvation and are located outside the localized high-concentration Li/DOL pairs or clusters. Ether solvents with high dielectric constants tightly wrap around the cation (see Figure S10 for solvation structures in DEGDME, TEGDME, and EEE), which can lead to shrinkage in volume of these solvents around Li^+ relative to that in the bulk solution. This so-called electrostriction[47] process can also extend to solvent molecules in the secondary solvation shell, reducing the available space for anionic species in the Li^+ solvation shell. Lastly, the previously mentioned properties of DTFEG, TFPG, and TFEG lead to a distinct top solvation structure compared with other fluorinated solvents in the ComBat dataset whereby these solvents participate in solvating Li^+ by contributing two coordinating oxygen atoms.

Clustering phenomena of the polysulfide

Li_2S_8 monomer units readily form dynamic clusters in the DOL/solvent electrolyte systems. Figure 4A shows the distribution of $(Li_2S_8)_s$ cluster sizes in each system averaged over the respective classical CMD trajectories over time. The rows in the table are arranged in an ascending order of $P_{s=1}$ within each solvent class, i.e., Li_2S_8 polysulfide clustering increases moving downward. The probability of forming a polysulfide of cluster size s (P_s), averaged over all the electrolyte systems, follows a decaying exponential function[48] of the form $Const.e^{-s/M}$ with a characteristic decay number M ~0.7 (Figure 4B). Representative clusters of each size are shown in Figure 4C. The cluster size distribution indicates that single polysulfide monomers prevail in the solution, with the tetramer $(Li_2S_8)_4$ being the largest cluster formed. Clearly, the aggregation of long-chain Li_2S_8 is strongly dependent on the solvent type. Figure 4A shows that, in general, a positive correlation exists between the bridging extent and the probability of forming larger Li_2S_8 clusters within each solvent class. The bridging extent is a quantitative property representing the fraction of Li^+ ions coordinating with more than one polysulfide species in their first solvation shell. Overall, greater bridging extents are accompanied with lower probabilities of Li_2S_8 monomeric units and impeded polysulfide dissolution. Additionally, a loose positive correlation exists between the solvent - Li_2S_8 binding affinity and the degree of polysulfide clustering within each solvent chemical class. Lower binding affinities often lead to higher probabilities of forming larger polysulfide aggregates.

The lowest polysulfide solubilities are achieved in fluorinated-, nonpolar-, silane-, and sulfide-containing electrolytes, in agreement with the non-solvating properties of these solvents discussed earlier. Within the ether class, MTBE, DIPE, DBE, and EPE result in the lowest polysulfide solubility, consistent with previous recordings that the room temperature solubility of Li_2S_8 is ~0.5 M in DOL/DME,[49] while it is only 20 mM in MTBE[50] and 4 mM in DIPE.[51] The most significant bridging occurs in the fluorinated FDE-based electrolyte, resulting in the agglomeration of Li_2S_8 into separate and well-defined domains, as shown in Figure S7C. This enduring Li_2S_8 clustering network limits the solubility of the polysulfides ($P_{s=1}$ = 0.35), thus reducing sulfur loss and shuttle effects. We hypothesize that the clustering and aggregation of polysulfides in such fluorinated electrolytes is responsible for the quasi-solid-state reaction kinetics reported previously compared with the dominant solution pathway in DOL/DME electrolytes.[8,52] Conversely, the electrolyte composed of the high-polarity DMSO solvent is the most vulnerable to polysulfide shuttle effects ($P_{s=1}$ = 0.97) due to a combination of two factors: (1) limited polysulfide bridging effect ($P_{bridging}$ = 0.003) and (2) availability of free solvent to solvate the cation. These factors prevent agglomeration of Li_2S_8 into separate domains and results in the polysulfides becoming much more evenly distributed in the simulation box (Figure S7A). This observation is in line with previous reports that lower-order polysulfides favor clustering while higher-order species prefer monomeric units in DMSO.[53] Sulfone-based electrolytes such as those containing SL and 2-(methyl sulphonyl)propane (IPMS) exhibit bridging extents and

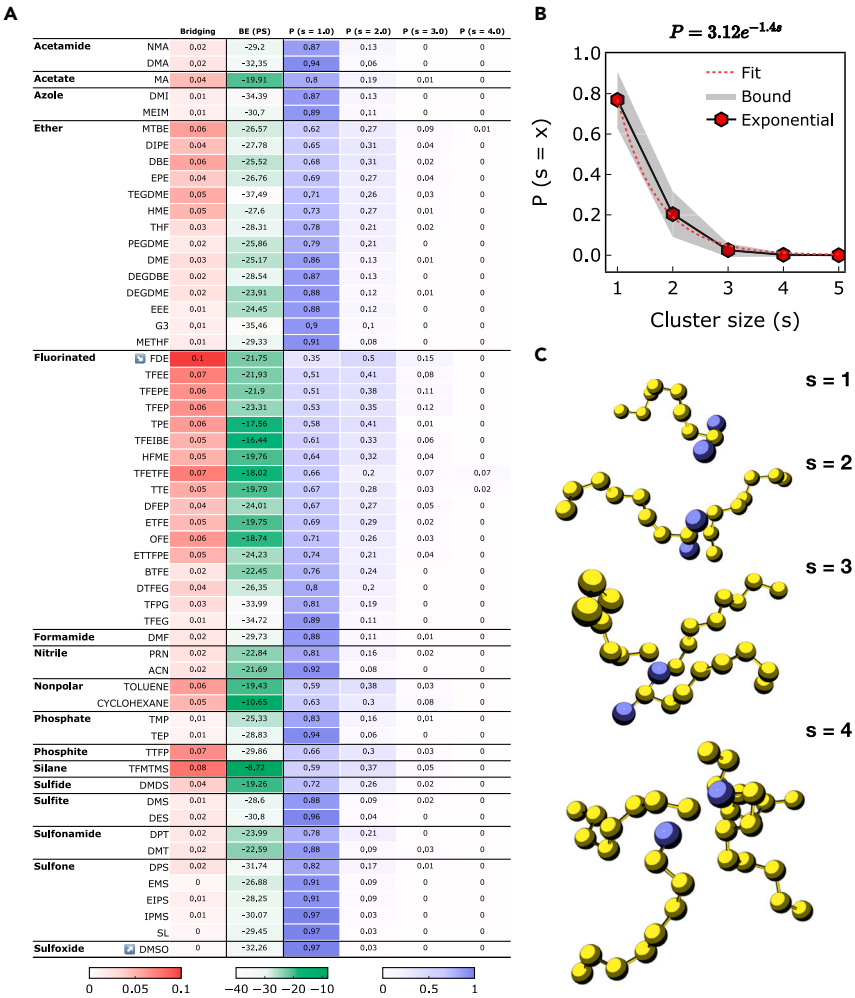

		Bridging	BE (PS)	P (s = 1.0)	P (s = 2.0)	P (s = 3.0)	P (s = 4.0)
Acetamide	NMA	0.02	-29.2	0.87	0.13	0	0
	DMA	0.02	-32.35	0.94	0.06	0	0
Acetate	MA	0.04	-19.91	0.8	0.19	0.01	0
Azole	DMI	0.01	-34.39	0.87	0.13	0	0
	MEIM	0.01	-30.7	0.89	0.11	0	0
Ether	MTBE	0.06	-26.57	0.62	0.27	0.09	0.01
	DIPE	0.04	-27.78	0.65	0.31	0.04	0
	DBE	0.06	-25.52	0.68	0.31	0.02	0
	EPE	0.04	-26.76	0.69	0.27	0.04	0
	TEGDME	0.05	-37.49	0.71	0.26	0.03	0
	HME	0.05	-27.6	0.73	0.27	0.01	0
	THF	0.03	-28.31	0.78	0.21	0.02	0
	PEGDME	0.02	-25.86	0.79	0.21	0	0
	DME	0.03	-25.17	0.86	0.13	0.01	0
	DEGDBE	0.02	-28.54	0.87	0.13	0	0
	DEGDME	0.02	-23.91	0.88	0.12	0.01	0
	EEE	0.01	-24.45	0.88	0.12	0	0
	G3	0.01	-35.46	0.9	0.1	0	0
	METHF	0.01	-29.33	0.91	0.08	0	0
Fluorinated	FDE	0.1	-21.75	0.35	0.5	0.15	0
	TFEE	0.07	-21.93	0.51	0.41	0.08	0
	TFEPE	0.06	-21.9	0.51	0.38	0.11	0
	TFEP	0.06	-23.31	0.53	0.35	0.12	0
	TPE	0.06	-17.56	0.58	0.41	0.01	0
	TFEIBE	0.05	-16.44	0.61	0.33	0.06	0
	HFME	0.05	-19.76	0.64	0.32	0.04	0
	TFETFE	0.07	-18.02	0.66	0.2	0.07	0.07
	TTE	0.05	-19.79	0.67	0.28	0.03	0.02
	DFEP	0.04	-24.01	0.67	0.27	0.05	0
	ETFE	0.05	-19.75	0.69	0.29	0.02	0
	OFE	0.06	-18.74	0.71	0.26	0.03	0
	ETTFPE	0.05	-24.23	0.74	0.21	0.04	0
	BTFE	0.02	-22.45	0.76	0.24	0	0
	DTFEG	0.04	-26.35	0.8	0.2	0	0
	TFPG	0.03	-33.99	0.81	0.19	0	0
	TFEG	0.01	-34.72	0.89	0.11	0	0
Formamide	DMF	0.02	-29.73	0.88	0.11	0.01	0
Nitrile	PRN	0.02	-22.84	0.81	0.16	0.02	0
	ACN	0.02	-21.69	0.92	0.08	0	0
Nonpolar	TOLUENE	0.06	-19.43	0.59	0.38	0.03	0
	CYCLOHEXANE	0.05	-10.65	0.63	0.3	0.08	0
Phosphate	TMP	0.01	-25.33	0.83	0.16	0.01	0
	TEP	0.01	-28.83	0.94	0.06	0	0
Phosphite	TTFP	0.07	-29.86	0.66	0.3	0.03	0
Silane	TFMTMS	0.08	-8.72	0.59	0.37	0.05	0
Sulfide	DMDS	0.04	-19.26	0.72	0.26	0.02	0
Sulfite	DMS	0.01	-28.6	0.88	0.09	0.02	0
	DES	0.02	-30.8	0.96	0.04	0	0
Sulfonamide	DPT	0.02	-23.99	0.78	0.21	0	0
	DMT	0.02	-22.59	0.88	0.09	0.03	0
Sulfone	DPS	0.02	-31.74	0.82	0.17	0.01	0
	EMS	0	-26.88	0.91	0.09	0	0
	EIPS	0.01	-28.25	0.91	0.09	0	0
	IPMS	0.01	-30.07	0.97	0.03	0	0
	SL	0	-29.45	0.97	0.03	0	0
Sulfoxide	DMSO	0	-32.26	0.97	0.03	0	0

0 0.05 0.1 −40 −30 −20 −10 0 0.5 1

Figure 4. Polysulfide clustering analysis for the electrolytes in the ComBat dataset

(A) Probability of the bridging effect, binding energy of the solvent with Li_2S_8 (kcal/mol), and probability of different polysulfide cluster sizes. (B) Average probability of cluster sizes in the entire dataset along with the fitted exponential function, and (C) representative polysulfide clusters formed in the electrolytes.

polysulfide solubilities on the same order of magnitude as those in the DMSO system. For these reasons, SL has been used in a small volume ratio when combined with DOL/DME[23] or in an equivolume mixture with a fluorinated solvent.[25] The high polysulfide solubility in sulfone systems can be explained by considering that SL is a strong Lewis acid while Li_2S_8 is a Lewis base leading to strong interactions between these two components. It has been experimentally confirmed that SL can even dissolve Li_2S by one order of magnitude higher than DOL and DME, thus playing the dual role of controlling the Li_2S deposition on the cathode and improving the stability of the Li anode by acting as an SEI film-forming additive.[23] On the contrary, the electrochemically active dimethyl disulfide (DMDS) solvent[54] is a Lewis base, similar to polysulfides, which weakens the solvent-polysulfide interactions and reduces the polysulfide solubility ($P_{s=1}$ = 0.72 in DMDS compared with 0.97 in SL). We finally note that no simple, direct, or monotonic relationship was found between the dielectric constant, donor number, C/O, fluorination degree, or other relevant solvent properties and the polysulfide solubilities as is often suggested in the literature. Instead, the observed trends are the collective result of an intricate interplay between these critical metrics. Thus, one should carefully consider as many metrics as possible when selecting a candidate solvent for Li-S batteries.

Dynamics of the electrolyte

Next, we investigated the diffusion mechanism of the electrolyte species as a function of the solvent type. To do that, we introduced a quantitative metric termed $P_{overlap}$ that describes the probability of overlap between the distribution of the diffusion coefficients of the Li^+ ion and each of the polysulfide and the solvent (see supplemental information for a detailed description). $P_{overlap}$ is normalized to yield a value between zero and one. A value of zero indicates no overlap between the two diffusion distributions, while a value of unity indicates similar distributions. Figures 5A–5C show the dependence of the average self-diffusion coefficients of Li^+, S_8^{2-}, and $TFSI^-$, respectively, on $P_{overlap}$ with S_8^{2-} (x axis) and the solvent (color bar) for all the electrolyte systems in the ComBat dataset. The relation between the diffusion coefficients of the ionic species and $P_{overlap}$ with S_8^{2-} is well described by an exponential function. Higher overlap is associated with slower diffusion of all ionic species. However, as is discussed later, high overlap does not always imply that the motion of Li^+ and the polysulfide is correlated.

Four distinct modes of diffusion are observed in the ComBat dataset (see Table S11 for the categorization of the solvents based on their diffusion mode). Electrolytes in group A (highlighted in yellow in Figures 5A–5C) exhibit high $P_{overlap}$ with both the solvent and the polysulfide and slow ionic dynamics. A closer inspection of the data reveals that this behavior is mainly a characteristic of the phosphate-, phosphite-, sulfonamide-, sulfone-, and sulfoxide-containing electrolytes. The slow dynamics in these electrolytes is attributed to the high viscosity of the solvents[23,36,55,56] and/or the tendency of Li^+ to aggregate into clusters or networks of Li^+ ions bound by shared or bridging solvent molecules. An example of the distribution of diffusion coefficients in these systems is shown in Figure 5D for a 1,1,1-trifluoro-N,N-dimethylmethane sulfonamide (DMT)-based electrolyte (refer to Figures S12 and S13 for distributions of the full dataset). Starting with the boxplots, we find that the diffusion coefficients of DOL are significantly higher than those of the other electrolyte species, indicating that most DOL molecules exist in the "free" state in the solution. This is evident from the weak Li^+ - DOL interactions in these systems as shown in the RDFs

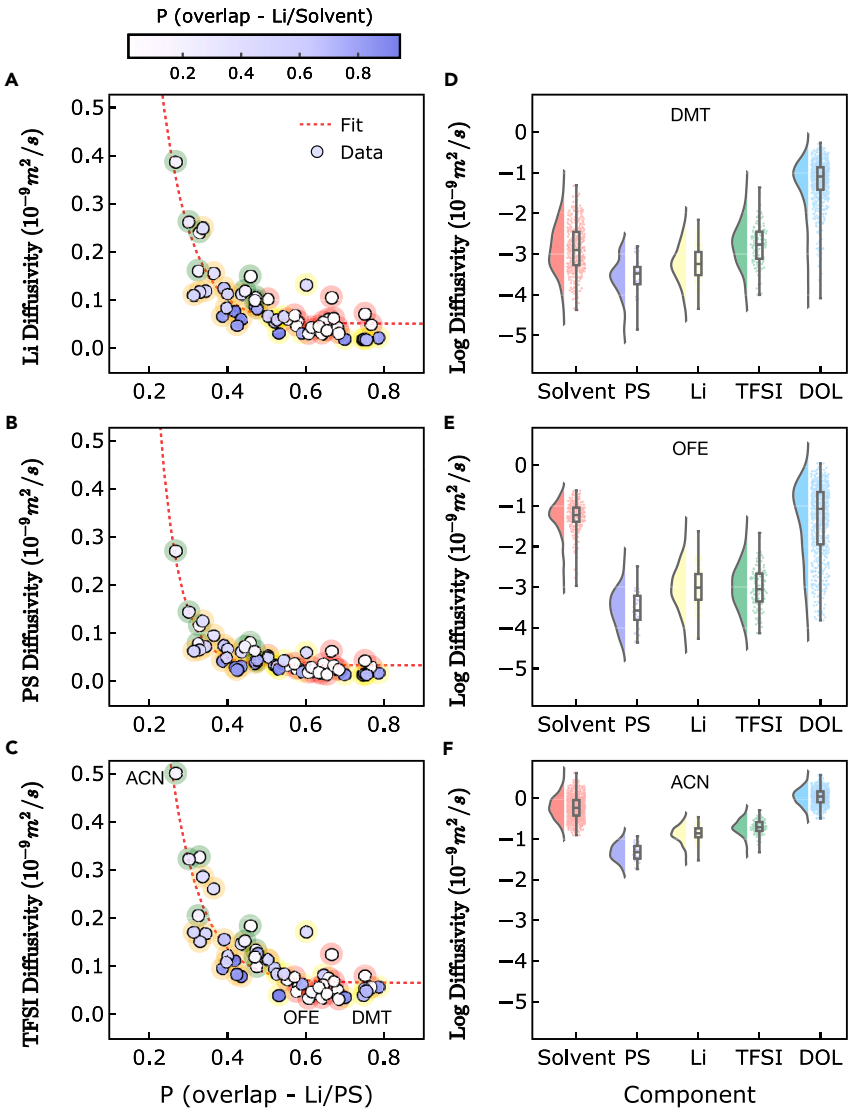

Figure 5. Dynamics of the Li^+ electrolytes in the ComBat dataset

Self-diffusion coefficients of (A) Li^+, (B) S_8^{2-}, and (C) $TFSI^-$ as a function of the probability of overlapping diffusivities between Li^+ and S_8^{2-} (PS). The color bar reflects the probability of overlapping diffusivities between Li^+ and the solvent used in each electrolyte system. The yellow, red, orange, and green boundary colors are indicative of electrolyte groups A to D, respectively. Raincloud plots (i.e., combined violin, box, and strip plots) for the CMD-computed diffusion coefficients of the solvent, S_8^{2-}, Li^+, $TFSI^-$, and DOL in (D) DMT-, (E) OFE-, and (F) ACN-containing electrolytes reflecting the unique diffusion behaviors of the electrolytes in the ComBat dataset. The strip plots show all the diffusion data for each electrolyte component. In the boxplots, the whisker tails correspond to the extrema, the boundaries correspond to the interquartile range, and the horizontal line corresponds to the median. The violin plots show the probability density of the diffusion coefficients of each electrolyte component. An interactive plot is hosted on GitHub at https://rashatwi.github.io/combat/plots/diffusion.html.

in Figure S4. When comparing the violin plots in Figure 5D, it is immediately clear that the shape of the diffusion coefficients distribution is dependent on the electrolyte component. The Li^+, polysulfide, and solvent distributions exhibit significant overlap, providing a visual representation of the high $\boldsymbol{P_{overlap}}$ values in these electrolytes. The high $\boldsymbol{P_{overlap}}$ of Li^+ with the polysulfide in the systems of group A is not caused by the correlated motion of the two species but rather by the slow overall dynamics, causing the ionic species to move at a similar pace. Because the rate capability of a cell is determined by the solvation and dissociation of ionic compounds and their subsequent migration through the solvent media, the electrolyte viscosity is an important metric for cell manufacturing rate. Thus, we also investigated the impact of the solvent type on the viscosity (Figure 6). Electrolytes in group A display viscosities that are between 1.7 and 6.4 higher than that in a DOL/DME system, which correlates with the low ion mobility in these solvents.

Group B is also characterized with slow ionic transport but $\boldsymbol{P_{overlap}}$ that is high with the polysulfide but low with the solvent (highlighted in red in Figures 5A–5C). This type of diffusion occurs mostly in nonpolar-, silane-, and fluorinated-based electrolytes excluding DTFEG, TFPG, and TFEG systems. Figure 5E, corresponding to an OFE-based electrolyte, shows that there is almost no overlap between the distribution of diffusion coefficients of the solvent and that of Li^+ and $\boldsymbol{S_8^{2-}}$ in such systems. The ratio of the average self-diffusion coefficient of the solvent to that of Li^+ ($\frac{D_{solvent}}{D_{Li^+}}$) is estimated to range between 6 and 23, which confirms that these solvents exist as free molecules and do not participate in coordinating with Li^+. The formation of n-AGGs composed of Li^+ and $\boldsymbol{S_8^{2-}}$ ions is the origin of the slow transport of ions. Once the clusters are formed, the displacements of Li^+ and polysulfides are restricted to localized motion within or around these n-AGGs. The diffusion of Li^+ ions through the n-AGGs relies on the structural motion, i.e., diffusion of ions through successive dissociation/association exchange across labile coordination structures.[8] This mode of diffusion is evident from the short Li^+ residence time with the solvent (Figures S14 and S15). Given that the clusters are relatively immobile, the local motion of Li^+ ions can barely contribute to long-range charge transport. Ionic conductivity studies of these electrolytes composed of 1 M LiTFSI in DOL/co-solvent (1/1, v/v) also display values that are, on average, between 5.4 and 16.4 times lower than that in the DOL/DME system (Figure 6). Such drastic conductivity losses are caused by CIP formation and slower ionic mobility in systems of group B. The data presented here are consistent with the dynamical behavior observed experimentally for fluorinated solvent-containing electrolytes[58,60] and highlights the need for strategies that can achieve optimal polysulfide solubility without significantly compromising the transport properties. It is also worth noting that although the viscosities of systems in group B are lower

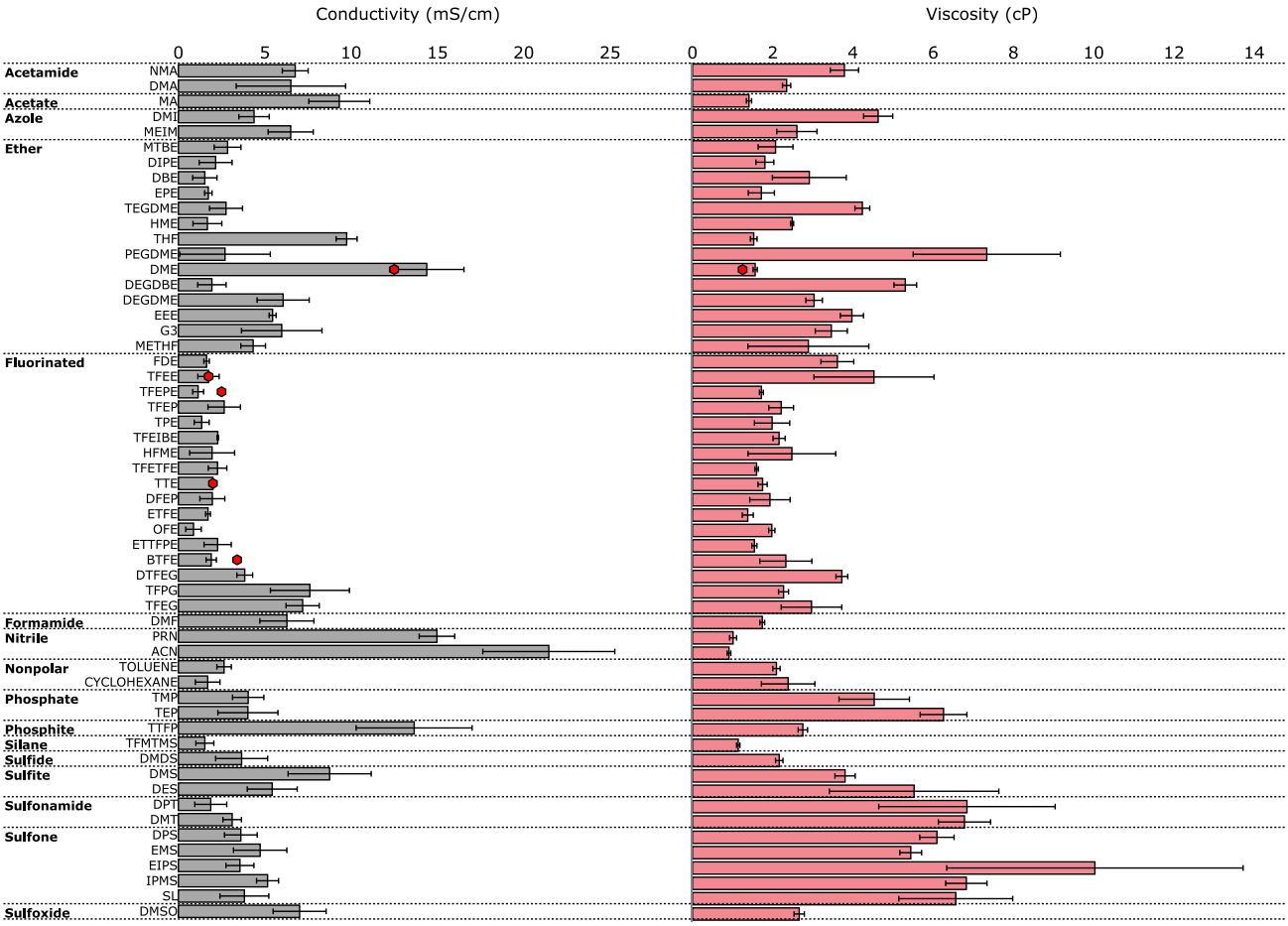

Figure 6. Ionic conductivity and viscosity of the electrolytes in the ComBat dataset

Horizontal bars correspond to CMD-computed properties for electrolytes composed of 1 M LiTFSI in DOL/co-solvent (1/1, v/v) with error bars representing standard deviation. Red hexagons correspond to experimentally reported values from the following references: DME-based electrolyte viscosity[57] DME and TFEE electrolytes conductivity[58] and TTE, TFEPE, and BTFE electrolytes conductivity.[59] An interactive plot is hosted on GitHub at https://rashatwi.github.io/combat/plots/visc_cond.html.

than those in group A (Figure 6), the ionic conductivities of the latter are higher due to their higher ionic dissociation degree.

Group C (highlighted in orange in Figures 5A–5C) includes acetamide-, formamide-, sulfite-, TFEG, and TFPG fluorinated systems, and many ether solvents such as DME, DEGDME, and TEGDME. These systems are characterized with $\boldsymbol{P_{overlap}}$ that is low with the polysulfides but high with the solvents. The origin of this diffusion behavior is attributed to the formation of long-lived solvation shells composed of solvent molecules tightly wrapped around the cations. For example, the residence time of DME in the cation solvation shell is 5.4 ns compared with only 14 ps in the OFE electrolyte (Figure S15A). Furthermore, $\frac{D_{solvent}}{D_{Li^+}}$ varies between 1.1 and 1.7 in these systems, suggesting that the Li^+ ions drift appreciably with their neighboring solvents through vehicular motion in the form of positively charged complexes, which is in agreement with previously reported experimental evidence.[45] We also note the presence of two peaks in the diffusion coefficient distribution of TFEG and TFPG solvents (Figure S13). This observation indicates the presence of two distinct groups of TFEG and TFPG molecules. The first group corresponds to fast solvents that exist as free molecules, and the other represents slow solvents that participate in the first solvation shell of the cation.

Last, systems of group D are characterized with the highest ionic diffusion coefficients and low $\boldsymbol{P_{overlap}}$ with both the solvent and the polysulfide (highlighted in green in Figures 5A–5C). This mode of diffusion occurs in the acetate, nitrile, sulfide, and some ether-containing electrolytes such as THF and 2-methyl tetrahydrofuran (METHF). Figure 5F, corresponding to an ACN-based electrolyte, shows that there is almost no overlap between the distribution of diffusion coefficients of Li^+ and that of the solvent and of $\boldsymbol{S_8^{2-}}$ in such systems. The fast dynamics here are attributed to the low viscosity of the solvents[36,61] and/or the dominant structural diffusion where the neighboring species do not diffuse together by a substantial amount. For instance, the ACN exchange rate around the cation is more than six times faster than that of DME (Figure S15).

Conclusion

In this work, we have developed a database coined ComBat of quantum-chemical and molecular dynamics properties for Li-S

electrolytes via a high-throughput multi-scale computational infrastructure.[29] The electrolytes included in the database consist of 1 M LiTFSI and 0.25 M Li_2S_8 in DOL/co-solvent (1/1, v/v). The co-solvents span 16 chemical classes that have been previously reported in Li-S literature. DFT-computed geometries, binding energies, RDFs, coordination numbers, diffusion coefficients, solvation structures, polysulfide clusters, viscosities, ionic conductivities, and electrolyte configurations are made publicly available.

We used the ComBat database to develop a fundamental understanding of the molecular origins of the reported behavior in these electrolyte formulations. We found a positive correlation between the degree of Li^+ ion dissociation from the polysulfides and the binding affinity of the solvent with the salt and the polysulfide. Ion dissociation is a critical property that impacts the ionic conductivity and thus the electrochemical performance of the battery. We also investigated the structural properties and the diffusion mechanism of the electrolyte species. Direct comparisons of diffusion coefficients for a relatively large dataset of solvents spanning different chemical classes are unlikely to result in meaningful trends and correlations. To overcome this challenge, we introduced a quantitative metric that describes the probability of overlap between the distribution of the diffusion coefficients of two electrolyte species. Using this metric, we classified the Li-S solvents in the ComBat database into four groups. We correlated the predicted ensemble properties in each group to the solvent properties.

Last, we note that the ComBat database is a living resource and several updates to the database are planned. For example, similar systematic studies will be performed in the future to include the effect of anions, additives, and various polysulfide chain lengths. We also plan to include other relevant properties such as redox potentials, bond dissociation energies, and transference numbers and study the effect of the solvent volumetric ratio. With all this in mind, we envision that our work will be used to inform and explore viable paths forward to optimize the composition of solvent mixtures used in Li-S electrolytes.

EXPERIMENTAL PROCEDURES

Resource availability

Lead contact

Further information and requests for resources and materials should be directed to and will be fulfilled by the lead contact, Nav Nidhi Rajput (navnidhi.rajput@stonybrook.edu).

Materials availability

This study did not generate new, unique reagents.

Data and code availability

Other than Gaussian and LAMMPS, all the necessary code used to generate and analyze the Li-S dataset (MISPR for workflow management: https://github.com/molmd/mispr; MDPropTools: for CMD analysis https://github.com/molmd/mdproptools; pymatgen for molecule representation and file i/o handling: https://github.com/molmd/pymatgen/tree/molmd_fix; and custodian for automatic error handling: https://github.com/molmd/custodian) can be found on GitHub. The ComBat dataset described in this work is made publicly available at GitHub (https://github.com/rashatwi/combat) and Zenodo: https://doi.org/10.5281/zenodo.7830272.[31]

SUPPLEMENTAL INFORMATION

Supplemental information can be found online at https://doi.org/10.1016/j.patter.2023.100799.

ACKNOWLEDGMENTS

The authors acknowledge funding from LG Energy Solutions. R.A. acknowledges support via a Junior Research Award from the Institute for Advanced Computational Science (IACS) at Stony Brook University. The authors also acknowledge computing resources from IACS.

AUTHOR CONTRIBUTIONS

Conceptualization, R.A. and N.N.R.; Methodology, software, validation, formal analysis, investigation, data curation, writing – original draft, visualization, R.A.; Writing – reviewing & editing, R.A. and N.N.R.; Supervision, project administration, and funding acquisition, N.N.R.

DECLARATION OF INTERESTS

The authors declare no competing interests.

Received: December 15, 2022
Revised: April 21, 2023
Accepted: June 21, 2023
Published: July 25, 2023

REFERENCES

1. Nitta, N., Wu, F., Lee, J.T., and Yushin, G. (2015). Li-ion battery materials: present and future. Mater. Today *18*, 252–264. https://doi.org/10.1016/j.mattod.2014.10.040.
2. Li, Y., and Guo, S. (2021). Material design and structure optimization for rechargeable lithium-sulfur batteries. Matter *4*, 1142–1188. https://doi.org/10.1016/j.matt.2021.01.012.
3. Liu, K., Liu, Y., Lin, D., Pei, A., and Cui, Y. (2018). Materials for lithium-ion battery safety. Sci. Adv. *4*, eaas9820. https://doi.org/10.1126/sciadv.aas9820.
4. Manthiram, A., Chung, S.H., and Zu, C. (2015). Lithium–sulfur batteries: progress and prospects. Adv. Mater. *27*, 1980–2006. https://doi.org/10.1002/adma.201405115.
5. Shen, Z., Zhang, W., Mao, S., Li, S., Wang, X., and Lu, Y. (2021). Tailored Electrolytes Enabling Practical Lithium–Sulfur Full Batteries via Interfacial Protection. ACS Energy Lett. *6*, 2673–2681. https://doi.org/10.1021/acsenergylett.1c01091.
6. Bruce, P.G., Freunberger, S.A., Hardwick, L.J., and Tarascon, J.-M. (2011). Li–O2 and Li–S batteries with high energy storage. Nat. Mater. *11*, 19–29. https://doi.org/10.1038/nmat3191.
7. Manthiram, A., Fu, Y., and Su, Y.-S. (2013). Challenges and prospects of lithium–sulfur batteries. Acc. Chem. Res. *46*, 1125–1134. https://doi.org/10.1021/ar300179v.
8. Yu, Z., Balsara, N.P., Borodin, O., Gewirth, A.A., Hahn, N.T., Maginn, E.J., Persson, K.A., Srinivasan, V., Toney, M.F., Xu, K., et al. (2021). Beyond Local Solvation Structure: Nanometric Aggregates in Battery Electrolytes and Their Effect on Electrolyte Properties. ACS Energy Lett. *7*, 461–470. https://doi.org/10.1021/acsenergylett.1c02391.
9. Zhao, M., Li, B.Q., Peng, H.J., Yuan, H., Wei, J.Y., and Huang, J.Q. (2020). Lithium–sulfur batteries under lean electrolyte conditions: challenges and opportunities. Angew. Chem. Int. Ed. Engl. *59*, 12636–12652. https://doi.org/10.1002/anie.201909339.
10. Zhang, L., Liu, D., Muhammad, Z., Wan, F., Xie, W., Wang, Y., Song, L., Niu, Z., and Chen, J. (2019). Single nickel atoms on nitrogen-doped graphene enabling enhanced kinetics of lithium–sulfur batteries. Adv. Mater. *31*, 1903955. https://doi.org/10.1002/adma.201903955.
11. Wu, F., Chen, S., Srot, V., Huang, Y., Sinha, S.K., van Aken, P.A., Maier, J., and Yu, Y. (2018). A Sulfur–Limonene-Based Electrode for Lithium–Sulfur Batteries: High-Performance by Self-Protection. Adv. Mater. *30*, 1706643. https://doi.org/10.1002/adma.201706643.
12. Wu, F., Lee, J.T., Fan, F., Nitta, N., Kim, H., Zhu, T., and Yushin, G. (2015). A Hierarchical Particle–Shell Architecture for Long-Term Cycle Stability of

Li2S Cathodes. Adv. Mater. *27*, 5579–5586. https://doi.org/10.1002/adma.201502289.

13. Wild, M., and Offer, G.J. (2019). Lithium-sulfur Batteries (John Wiley & Sons).
14. Chen, J., Han, K.S., Henderson, W.A., Lau, K.C., Vijayakumar, M., Dzwiniel, T., Pan, H., Curtiss, L.A., Xiao, J., Mueller, K.T., et al. (2016). Restricting the Solubility of Polysulfides in Li-S Batteries Via Electrolyte Salt Selection. Adv. Energy Mater. *6*, 1600160. https://doi.org/10.1002/aenm.201600160.
15. Rajput, N.N., Murugesan, V., Shin, Y., Han, K.S., Lau, K.C., Chen, J., Liu, J., Curtiss, L.A., Mueller, K.T., and Persson, K.A. (2017). Elucidating the solvation structure and dynamics of lithium polysulfides resulting from competitive salt and solvent interactions. Chem. Mater. *29*, 3375–3379. https://doi.org/10.1021/acs.chemmater.7b00068.
16. Zu, C., Azimi, N., Zhang, Z., and Manthiram, A. (2015). Insight into lithium–metal anodes in lithium–sulfur batteries with a fluorinated ether electrolyte. J. Mater. Chem. A Mater. *3*, 14864–14870. https://doi.org/10.1039/C5TA03195H.
17. Cheng, L., Curtiss, L.A., Zavadil, K.R., Gewirth, A.A., Shao, Y., and Gallagher, K.G. (2016). Sparingly solvating electrolytes for high energy density lithium–sulfur batteries. ACS Energy Lett. *1*, 503–509. https://doi.org/10.1021/acsenergylett.6b00194.
18. Azimi, N., Xue, Z., Bloom, I., Gordin, M.L., Wang, D., Daniel, T., Takoudis, C., and Zhang, Z. (2015). Understanding the effect of a fluorinated ether on the performance of lithium–sulfur batteries. ACS Appl. Mater. Interfaces *7*, 9169–9177. https://doi.org/10.1021/acsami.5b01412.
19. Azimi, N., Weng, W., Takoudis, C., and Zhang, Z. (2013). Improved performance of lithium–sulfur battery with fluorinated electrolyte. Electrochem. Commun. *37*, 96–99. https://doi.org/10.1016/j.elecom.2013.10.020.
20. Gordin, M.L., Dai, F., Chen, S., Xu, T., Song, J., Tang, D., Azimi, N., Zhang, Z., and Wang, D. (2014). Bis (2, 2, 2-trifluoroethyl) ether as an electrolyte co-solvent for mitigating self-discharge in lithium–sulfur batteries. ACS Appl. Mater. Interfaces *6*, 8006–8010. https://doi.org/10.1021/am501665s.
21. Azimi, N., Xue, Z., Rago, N.D., Takoudis, C., Gordin, M.L., Song, J., Wang, D., and Zhang, Z. (2014). Fluorinated electrolytes for Li-S battery: suppressing the self-discharge with an electrolyte containing fluoroether solvent. J. Electrochem. Soc. *162*, A64–A68. https://doi.org/10.1149/2.0431501jes.
22. Yoon, S., Lee, Y.-H., Shin, K.-H., Cho, S.B., and Chung, W.J. (2014). Binary sulfone/ether-based electrolytes for rechargeable lithium-sulfur batteries. Electrochim. Acta *145*, 170–176. https://doi.org/10.1016/j.electacta.2014.09.007.
23. Liu, Y., Pan, Y., Ban, J., Li, T., Jiao, X., Hong, X., Xie, K., Song, J., Matic, A., and Xiong, S. (2020). Promoted rate and cycling capability of Li–S batteries enabled by targeted selection of co-solvent for the electrolyte. Energy Storage Mater. *25*, 131–136. https://doi.org/10.1016/j.ensm.2019.10.022.
24. Xu, K., and Angell, C.A. (2002). Sulfone-based electrolytes for lithium-ion batteries. J. Electrochem. Soc. *149*, A920. https://doi.org/10.1149/1.1483866.
25. Glaser, R., Borodin, O., Johnson, B., Jhulki, S., and Yushin, G. (2021). Minimizing Long-Chain Polysulfide Formation in Li-S Batteries by Using Localized Low Concentration Highly Fluorinated Electrolytes. J. Electrochem. Soc. *168*, 090543. https://doi.org/10.1149/1945-7111/ac2467.
26. Chen, J., Yang, H., Zhang, X., Lei, J., Zhang, H., Yuan, H., Yang, J., Nuli, Y., and Wang, J. (2019). Highly Reversible Lithium-Metal Anode and Lithium–Sulfur Batteries Enabled by an Intrinsic Safe Electrolyte. ACS Appl. Mater. Interfaces *11*, 33419–33427. https://doi.org/10.1021/acsami.9b09215.
27. Wang, J., Lin, F., Jia, H., Yang, J., Monroe, C.W., and NuLi, Y. (2014). Towards a safe lithium–sulfur battery with a flame-inhibiting electrolyte and a sulfur-based composite cathode. Angew. Chem. Int. Ed. Engl. *53*, 10099–10104. https://doi.org/10.1002/anie.201405157.
28. Cuisinier, M., Cabelguen, P.-E., Adams, B.D., Garsuch, A., Balasubramanian, M., and Nazar, L.F. (2014). Unique behaviour of nonsolvents for polysulphides in lithium–sulphur batteries. Energy Environ. Sci. *7*, 2697–2705. https://doi.org/10.1039/C4EE00372A.
29. Atwi, R., Bliss, M., Makeev, M., and Rajput, N.N. (2022). MISPR: an open-source package for high-throughput multiscale molecular simulations. Sci. Rep. *12*, 15760. https://doi.org/10.1038/s41598-022-20009-w.
30. Atwi, R., Chen, Y., Han, K.S., Mueller, K.T., Murugesan, V., and Rajput, N.N. (2022). An automated framework for high-throughput predictions of NMR chemical shifts within liquid solutions. Nat. Comput. Sci. *2*, 112–122. https://doi.org/10.1038/s43588-022-00200-9.
31. Atwi, R., and Rajput, N.N. (2023). The ComBat Database: A Database of Quantum-Chemical and Molecular Dynamics Properties for Li-S Electrolytes. https://doi.org/10.5281/zenodo.7830272.
32. Kim, S., Chen, J., Cheng, T., Gindulyte, A., He, J., He, S., Li, Q., Shoemaker, B.A., Thiessen, P.A., Yu, B., et al. (2023). PubChem 2023 update. Nucleic Acids Res. *51*, D1373–D1380. https://doi.org/10.1093/nar/gkac956.
33. Zou, Q., and Lu, Y.-C. (2016). Solvent-dictated lithium sulfur redox reactions: an operando UV–vis spectroscopic study. J. Phys. Chem. Lett. *7*, 1518–1525. https://doi.org/10.1021/acs.jpclett.6b00228.
34. Baek, M., Shin, H., Char, K., and Choi, J.W. (2020). New high donor electrolyte for lithium–sulfur batteries. Adv. Mater. *32*, 2005022. https://doi.org/10.1002/adma.202005022.
35. Li, Z., Zhou, Y., Wang, Y., and Lu, Y.C. (2019). Solvent-mediated Li2S electrodeposition: a critical manipulator in lithium–sulfur batteries. Adv. Energy Mater. *9*, 1802207. https://doi.org/10.1002/aenm.201802207.
36. He, Q., Gorlin, Y., Patel, M.U.M., Gasteiger, H.A., and Lu, Y.-C. (2018). Unraveling the correlation between solvent properties and sulfur redox behavior in lithium-sulfur batteries. J. Electrochem. Soc. *165*, A4027–A4033. https://doi.org/10.1149/2.0991816jes.
37. Guo, J., Xu, Y., and Wang, C. (2011). Sulfur-impregnated disordered carbon nanotubes cathode for lithium–sulfur batteries. Nano Lett. *11*, 4288–4294. https://doi.org/10.1021/nl202297p.
38. Weng, W., Pol, V.G., and Amine, K. (2013). Ultrasound assisted design of sulfur/carbon cathodes with partially fluorinated ether electrolytes for highly efficient Li/S batteries. Adv. Mater. *25*, 1608–1615. https://doi.org/10.1002/adma.201204051.
39. Zheng, J., Ji, G., Fan, X., Chen, J., Li, Q., Wang, H., Yang, Y., DeMella, K.C., Raghavan, S.R., and Wang, C. (2019). High-fluorinated electrolytes for Li–S batteries. Adv. Energy Mater. *9*, 1803774. https://doi.org/10.1002/aenm.201803774.
40. Gu, S., Qian, R., Jin, J., Wang, Q., Guo, J., Zhang, S., Zhuo, S., and Wen, Z. (2016). Suppressing the dissolution of polysulfides with cosolvent fluorinated diether towards high-performance lithium sulfur batteries. Phys. Chem. Chem. Phys. *18*, 29293–29299. https://doi.org/10.1039/C6CP04775K.
41. Yang, H.J., and Jung, Y. (2015). Effects of Polysulfide Nonsolvents on the Electrochemical Performance of Li-S Batteries. Int. J. Electrochem. Sci. *10*, 9049–9055. http://electrochemsci.org/papers/vol10/101109049.pdf.
42. Liu, T., Shi, Z., Li, H., Xue, W., Liu, S., Yue, J., Mao, M., Hu, Y.s., Li, H., Huang, X., et al. (2021). Low-Density Fluorinated Silane Solvent Enhancing Deep Cycle Lithium–Sulfur Batteries' Lifetime. Adv. Mater. *33*, 2102034. https://doi.org/10.1002/adma.202102034.
43. Berger, R., Resnati, G., Metrangolo, P., Weber, E., and Hulliger, J. (2011). Organic fluorine compounds: a great opportunity for enhanced materials properties. Chem. Soc. Rev. *40*, 3496–3508. https://doi.org/10.1039/C0CS00221F.
44. Fan, X., Ji, X., Chen, L., Chen, J., Deng, T., Han, F., Yue, J., Piao, N., Wang, R., Zhou, X., et al. (2019). All-temperature batteries enabled by fluorinated electrolytes with non-polar solvents. Nat. Energy *4*, 882–890. https://doi.org/10.1038/s41560-019-0474-3.
45. Zhang, S., Ueno, K., Dokko, K., and Watanabe, M. (2015). Recent advances in electrolytes for lithium–sulfur batteries. Adv. Energy Mater. *5*, 1500117. https://doi.org/10.1002/aenm.201500117.
46. Luo, D., Li, M., Zheng, Y., Ma, Q., Gao, R., Zhang, Z., Dou, H., Wen, G., Shui, L., Yu, A., et al. (2021). Electrolyte Design for Lithium Metal

Anode-Based Batteries Toward Extreme Temperature Application. Adv. Sci. *8*, 2101051. https://doi.org/10.1002/advs.202101051.

47. Marcus, Y. (2005). Electrostriction, ion solvation, and solvent release on ion pairing. J. Phys. Chem. B *109*, 18541–18549. https://doi.org/10.1021/jp051505k.
48. Israelachvili, J.N. (2011). Intermolecular and Surface Forces (Academic press).
49. Pan, H., Wei, X., Henderson, W.A., Shao, Y., Chen, J., Bhattacharya, P., Xiao, J., and Liu, J. (2015). On the way toward understanding solution chemistry of lithium polysulfides for high energy Li–S redox flow batteries. Adv. Energy Mater. *5*, 1500113. https://doi.org/10.1002/aenm.201500113.
50. Sun, K., Wu, Q., and Gan, H. (2018). Molecular insights into ether-based electrolytes for Li-FeS2 batteries. Energy Storage Mater. *12*, 85–93. https://doi.org/10.1016/j.ensm.2017.12.003.
51. Sun, K., Wu, Q., Tong, X., and Gan, H. (2018). Electrolyte with low polysulfide solubility for Li–S batteries. ACS Appl. Energy Mater. *1*, 2608–2618. https://doi.org/10.1021/acsaem.8b00317.
52. Lee, C.-W., Pang, Q., Ha, S., Cheng, L., Han, S.-D., Zavadil, K.R., Gallagher, K.G., Nazar, L.F., and Balasubramanian, M. (2017). Directing the lithium–sulfur reaction pathway via sparingly solvating electrolytes for high energy density batteries. ACS Cent. Sci. *3*, 605–613. https://doi.org/10.1021/acscentsci.7b00123.
53. Vijayakumar, M., Govind, N., Walter, E., Burton, S.D., Shukla, A., Devaraj, A., Xiao, J., Liu, J., Wang, C., Karim, A., and Thevuthasan, S. (2014). Molecular structure and stability of dissolved lithium polysulfide species. Phys. Chem. Chem. Phys. *16*, 10923–10932. https://doi.org/10.1039/C4CP00889H.
54. Chen, S., Dai, F., Gordin, M.L., Yu, Z., Gao, Y., Song, J., and Wang, D. (2016). Functional organosulfide electrolyte promotes an alternate reaction pathway to achieve high performance in lithium–sulfur batteries. Angew. Chem. Int. Ed. Engl. *55*, 4231–4235. https://doi.org/10.1002/anie.201511830.
55. Hilbig, P., Ibing, L., Wagner, R., Winter, M., and Cekic-Laskovic, I. (2017). Ethyl methyl sulfone-based electrolytes for lithium ion battery applications. Energies *10*, 1312. https://doi.org/10.3390/en10091312.
56. Feng, S., Huang, M., Lamb, J.R., Zhang, W., Tatara, R., Zhang, Y., Zhu, Y.G., Perkinson, C.F., Johnson, J.A., and Shao-Horn, Y. (2019). Molecular design of stable sulfamide-and sulfonamide-based electrolytes for aprotic Li-O2 batteries. Chem *5*, 2630–2641. https://doi.org/10.1016/j.chempr.2019.07.003.
57. Kim, H.-S., and Jeong, C.-S. (2011). Electrochemical properties of binary electrolytes for lithium-sulfur batteries. Bull. Kor. Chem. Soc. *32*, 3682–3686. https://doi.org/10.5012/bkcs.2011.32.10.3682.
58. Gao, M., Su, C., He, M., Glossmann, T., Hintennach, A., Feng, Z., Huang, Y., and Zhang, Z. (2017). A high performance lithium–sulfur battery enabled by a fish-scale porous carbon/sulfur composite and symmetric fluorinated diethoxyethane electrolyte. J. Mater. Chem. A Mater. *5*, 6725–6733. https://doi.org/10.1039/C7TA01057E.
59. Su, C.C., He, M., Amine, R., and Amine, K. (2019). A Selection Rule for Hydrofluoroether Electrolyte Cosolvent: Establishing a Linear Free-Energy Relationship in Lithium–Sulfur Batteries. Angew. Chem. *131*, 10701–10705. https://doi.org/10.1002/ange.201904240.
60. Yue, Z., Dunya, H., Aryal, S., Segre, C.U., and Mandal, B. (2018). Synthesis and electrochemical properties of partially fluorinated ether solvents for lithiumsulfur battery electrolytes. J. Power Sources *401*, 271–277. https://doi.org/10.1016/j.jpowsour.2018.08.097.
61. Ryu, H.S., Ahn, H.J., Kim, K.W., Ahn, J.H., Cho, K.K., Nam, T.H., Kim, J.U., and Cho, G.B. (2006). Discharge behavior of lithium/sulfur with TEGDME based electrolytes at low temperature. J. Power Sources *163*, 201–206. https://doi.org/10.1016/j.jpowsour.2005.12.061.